Article

Membrane Adhesion via Glycolipids Occurs for Abundant Saccharide Chemistries

Victoria M. Latza,[1] Bruno Demé,[2] and Emanuel Schneck[1,3,*]
[1]Biomaterials Department, Max Planck Institute of Colloids and Interfaces, Potsdam, Germany; [2]Institut Laue-Langevin, Grenoble, France; and [3]Physics Department, Technische Universität Darmstadt, Darmstadt, Germany

ABSTRACT Membrane-bound oligosaccharides with specific chemistries are known to promote tight adhesion between adjacent membranes via the formation of weak saccharide bonds. However, in the literature, one can find scattered evidence that other, more abundant saccharide chemistries exhibit similar behavior. Here, the influence of various glycolipids on the interaction between adjacent membranes is systematically investigated with the help of small- and wide-angle x-ray scattering and complementary neutron diffraction experiments. Added electrostatic repulsion between the membrane surfaces is used to identify the formation of saccharide bonds and to challenge their stability against tensile stress. Some of the saccharide headgroup types investigated are able to bind adjacent membranes together, but this ability has no significant influence on the membrane bending rigidity. Our results indicate that glycolipid-mediated membrane adhesion is a highly abundant phenomenon and therefore potentially of great biological relevance.

SIGNIFICANCE Biological membranes can contain considerable amounts of glycolipids. However, surprisingly little is known about the influence of glycolipids on the interaction between neighboring membranes, apart from a few special cases. Here, we find that various glycolipids with abundant types of saccharide headgroups are able to induce tight membrane adhesion even against repulsive forces, a phenomenon presumably playing important roles in cell biology.

INTRODUCTION

Biomembranes are vital components of all living organisms. They form the boundaries between the various compartments of cells and act as platforms for essential biochemical processes. But biomembranes do not only act alone, their functions being dependent on interactions with other membranes in their physiological environment. Membrane surfaces are formed by the headgroups of lipids and by membrane-bound saccharides, polypeptides, and other biomacromolecules (1). The interaction between membranes in their congested physiological surroundings is sensitive to this composition and affects the structural organization and function of membrane systems such as organelles, as well as membrane adhesion, vesicle release, and the formation of lamellar structures (2). Strikingly, naturally stacked membrane systems like myelin sheaths (3) or photosyn-

thetic membranes (thylakoids) in plants (4) contain high fractions of glycolipids. This correlation points toward a significant role of glycolipids in membrane adhesion. Indeed, early in vitro experiments with thylakoid lipid extracts (5) and glycolipids with a digalactose headgroup (*DGDG*) revealed spontaneous vesicle aggregation and membrane stack formation (6). Later on, the so-called hydration repulsion (i.e., the dehydrating pressure required to bring adjacent membranes to close proximity) was found to decay much more rapidly with the membrane separation for glycolipids (7,8) than for commonly studied phospholipids with phosphatidylcholine (PC) headgroups (9). These results are in agreement with an earlier study by Marra, who found that the adhesion energies between glycolipid bilayers are up to six times higher than for PC lipid bilayers (10,11). In contrast, Ricoul et al. reported that the addition of an uncharged glycolipid with a lactose headgroup appears to enhance the short-range repulsion between cationic surfactant lamellae (12). Wood et al. (13) investigated the interaction between PC lipid surfaces loaded with negatively charged glycolipids (sialo-gangliosides). Their results suggested repulsive saccharide interactions but favorable

interactions between the saccharides and PC. Recently, Kanduč et al. quantitatively reproduced the interaction characteristics of glycolipid and PC lipid membranes in solvent-explicit atomistic molecular dynamics simulations (14). The study revealed that the repulsion mechanisms responsible for the comparatively longer hydration repulsion range of PC lipid membranes are inoperative for the glycolipid membranes. On the basis of an interplay between long-range van der Waals attraction and hydration repulsion (15,16), the adhesion energy for the glycolipid membranes was thus estimated to be enhanced by a factor of approximately six with respect to PC lipid membranes (14), in excellent agreement with the results of Marra (10,11). Within this picture, the tight cohesion between glycolipid membranes is rationalized solely on the basis of a shorter-ranged hydration repulsion. In other words, it does not explicitly invoke attraction between the saccharide groups belonging to the opposing membrane surfaces. Other studies have, however, demonstrated that already small fractions of glycolipids can induce pronounced cohesion between lipid membranes. For example, attractive forces were measured between lipid vesicles displaying low surface densities of membrane-bound LewisX (17), a trisaccharide motif known to be involved in cell adhesion processes during embryonic development (18). Later on, neutron diffraction (ND) on membrane multilayers showed that LewisX lipids effectively cross-link adjacent membranes via favorable carbohydrate-carbohydrate interactions (in the following termed "saccharide bonds") even against repulsive membrane interactions (19). It was found that LewisX lipids lead to a strong confinement of the membrane separation around a value dictated by the lipids' saccharide headgroups. However, in the literature, one also finds indication that not only the spe-cific trisaccharide motif LewisX but also other motifs are able to cross-link membranes. Surprisingly strong attractive interactions were observed, for instance, for PC lipid membranes containing a glycolipid with a lactose disaccharide headgroup (N-hexadecanoyl-lactosylceramide, LacCer-sat) at ≈ 10 mol% (20). This finding is consistent with the observation that membrane-bound lactose has a similar effect on membrane adhesion as membrane-bound LewisX (17).

Here, we investigate how generic the phenomenon of membrane cross-linking by glycolipids is, i.e., to what extent it really depends on the chemical details of the saccharide headgroups. For this purpose, we study the interaction of stacked phospholipid membranes (Fig. 1 A) containing defined mole fractions of commercially available glycolipids with various types of uncharged saccharide headgroups. The headgroups feature a systematic increase in their length from mono- to tetrasaccharides (see Fig. 1 B) and comprise abundant monosaccharides (such as glucose and galactose) as their building blocks. Moreover, the glycolipid types investigated somewhat reflect the abundance and biological relevance of glycolipids in various organisms: mono- and digalactosyl-diglyceride (MGDG and DGDG, comprising one or two galactose units, respectively) are the main constituents of the thylakoid membranes of chloroplasts (4). Psychosine (Psyc) also comprises a single galactose unit. This glycosphingolipid is a derivative of galactocerebroside and abundant in the central nervous system of vertebrates (3). Lactosylceramide (Lac) with a lactose headgroup is associated with plentiful important functional roles in living cells, e.g., mediating the signal transduction pathway that leads to vascular endothelial cell proliferation (21–23). Ceramide-trihexoside (Trihexo) with a (galactose)-(galactose)-(glucose) headgroup is a glycosphingolipid involved
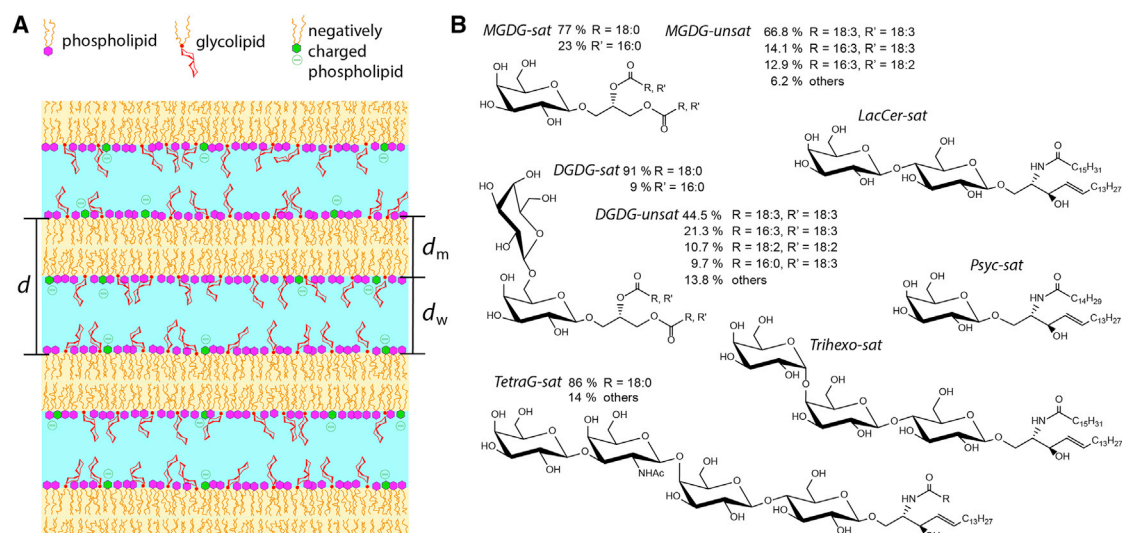

FIGURE 1 (A) A schematic illustration of phosphatidylcholine lipid membrane multilayers incorporating glycolipids and negatively charged phospholipids at various molar fractions. (B) The chemical structures of the glycolipids investigated are shown: LacCer-sat, MGDG-sat, MGDG-unsat, Psyc-sat, DGDG-sat, DGDG-unsat, Trihexo-sat, and TetraG-sat. To see this figure in color, go online.

in cellular signaling in mammals, in which it acts as a binding receptor for various toxins (24). Finally, gangliotetraosylceramide (*TetraG*) belongs to the asialo-gangliosides, a group of neutral glycosphingolipids, and is known to be a receptor for certain bacteria and toxins (25). Its saccharide headgroup is composed of (galactose)-(N-acetyl-galactose)-(galactose)-(glucose) (26). Regarding the hydrocarbon chains of the investigated glycolipids, we generally distinguish between predominantly saturated chains and predominantly unsaturated chains, indicated in the following and in Fig. 1 *B* with the suffices "*sat*" and "*unsat*," respectively. The influence of the glycolipids on the interaction between adjacent membranes is quantified with the help of small- and wide-angle x-ray scattering (SAXS/WAXS), which yield the lamellar period of the multilayers. To test the stability of the saccharide bonds against tensile stress, the membranes are further loaded with defined mole fractions of charged phospholipids, inducing controlled electrostatic repulsion between the membrane surfaces. We find that some of the saccharide headgroup types investigated are able to bind adjacent membranes together. For monosaccharides, no such cross-linking is observed, likely because they are too small to protrude from the headgroup layer of the matrix lipids. Overall, our results indicate that glycolipid-mediated membrane adhesion is a highly abundant phenomenon that is therefore potentially of great biological relevance.

MATERIALS AND METHODS

Chemicals

Unless stated otherwise the utilized chemicals were purchased from Sigma-Aldrich (St. Louis, MO) and used without further purification. Ultrapure water was used for all purposes (MilliQ grade). The phospholipids 1,2-dimyristoyl-*sn*-glycero-3-phosphocholine (DMPC), 1,2-dipalmitoyl-*sn*-glycero-3-phosphocholine (DPPC), 1-palmitoyl-2-oleoyl-*sn*-glycero-3-phosphocholine (POPC), 1,2-dimyristoyl-*sn*-glycero-3-phospho-(1'-rac-glycerol) (sodium salt) (DMPG), 1,2-dipalmitoyl-*sn*-glycero-3-phospho-(1'-rac-glycerol) (sodium salt) (DPPG), and 1-palmitoyl-2-oleoyl-*sn*-glycero-3-phospho-L-serine (sodium salt) (POPS) and the glycolipids digalactosyl-diacylglycerol unsaturated (*DGDG-unsat*) and monogalactosyl-diacylglycerol unsaturated (*MGDG-unsat*) were purchased from Avanti Polar Lipids (Alabaster, AL). The glycolipids digalactosyl-diacylglycerol saturated (*DGDG-sat*), monogalactosyl-diacylglycerol saturated (*MGDG-sat*), N-pentadecanoyl-psychosine (*Psyc-sat*), N-hexadecanoyl-lactosyl-ceramide (*LacCer-sat*), N-hexadecanoyl-ceramide-trihexoside (*Trihexo-sat*), and gangliotetraosyl-ceramide (*TetraG-sat*) were purchased from Matreya (State College, PA). The chain-melting temperatures of the phospholipids used as the matrix are summarized in Table 1.

Sample preparation

Before use, glassware was cleaned by 30 min immersion in chloroform, acetone, ethanol, water, and ethanol again and finally dried with a stream of nitrogen or argon. Aqueous buffers (based on H_2O or D_2O) contained 100 mM NaCl and 5 mM HEPES and were adjusted to pH 7 by the addition of 1 mM NaOH solution. Organic lipid solutions were prepared by weighing the lipid powder and adding solvent, resulting in a lipid concentration of

TABLE 1 Phase Transition Temperatures of the Phospholipids Used in This Study

Phospholipid	Transition Temperature (°C)
POPC	−2
POPS	14
DMPC	24
DMPG	23
DPPC	41
DPPG	41

Temperatures from (56).

2 mg/mL. Phospholipids were dissolved in chloroform and glycolipids in chloroform/methanol mixtures (4:1 or 2:1 v/v). Mixed lipid solutions were prepared by mixing defined volumes of the respective single-component lipid solutions. The mixtures were then dried in their original glass containers with a nitrogen stream for at least 3 h and subsequently exposed to vacuum overnight. To prepare suspensions of multilamellar lipid aggregates, aqueous buffer was added to the dry lipid mixtures. The suspensions were then first bath sonicated for 7 min, heated to ≈50°C for 1 h, and then stored at 5°C. Before the transfer into the measurement capillaries for SAXS/WAXS, the samples were again bath sonicated for 15 min. Each capillary was filled with 100 μL suspension and stored at 5°C overnight. For the preparation of solid-supported membrane multilayers, silicon wafers (size: 25 × 65 mm) were cleaned with the same protocol as the glassware. Shortly before deposition of the sample solution, the wafers were treated in an ultraviolet-ozone chamber for 20 min to activate the surface. A 0.5 mL volume of a 2 mg/mL lipid organic solution was placed on the polished face of the chip on a petri dish. To generate a homogenous multilayer covering most of the wafer surface, the petri dish was then manually rocked until all solvent was evaporated. The samples were then exposed to vacuum overnight to remove residual solvent and subsequently incubated for 3 h at 50°C and high D_2O humidity ($h_{rel} \geq 87\%$ (27), achieved by addition of 40 μL of a 1 M $BaCl_2$ solution in D_2O to the bottom of the Falcon tubes) for further annealing of the lamellar structures. Afterwards, they were stored in dry Falcon tubes at 5°C.

SAXS and WAXS

Combined SAXS and WAXS measurements were performed at the μSpot beamline (28) at Synchrotron Bessy II (Helmholtz-Zentrum Berlin, Berlin, Germany) with a beam energy of 15 keV corresponding to a wavelength of $\lambda = 0.0826$ nm. The beam was collimated with a set of pinholes with diameters of 100 and 150 μm, respectively. The x-ray scattering patterns were recorded with a position-sensitive two-dimensional (2D) detector, either MarMosaic 225 (Rayonix, Evanston) or Eiger X 9M (Dectris, Baden-Daetwil, Switzerland). The sample-to-detector distance was 480 mm. Measurements were conducted above the matrix lipid phase transition temperature (Table 1), either at 21°C (for samples based on POPC) or 50°C (for samples based on DMPC or DPPC). For this purpose, a home-made capillary holder with temperature control was used. The 2D scattering patterns obtained with the isotropically oriented multilamellar membrane aggregates (see Fig. 2 *A* for an example) are radially symmetrical to good approximation (powder limit) and were thus integrated in the azimuthal direction to obtain one-dimensional intensity profiles as a function of the magnitude q of the scattering vector (radial plot), $q = (4\pi/\lambda)\sin(\Gamma/2)$, associated with the scattering angle Γ. This procedure was performed with the software DPDAK (29), which also provides a precise q axis calibration based on silver behenate ($CH_3(CH_2)_{20}COOAg$) as the calibration standard. The intensity profiles $I(q)$ exhibit a number of Bragg peaks in the small-angle range (see Fig. 2 *B*), whose q-positions are related to the lamellar period d of the membrane multilayers according to Bragg's law, $q_{peak} = 2\pi n/d$, where n (= 1, 2, ...) is the diffraction order. The precise peak positions were determined via Gaussian fits including an adjustable flat background. As shown in the inset of
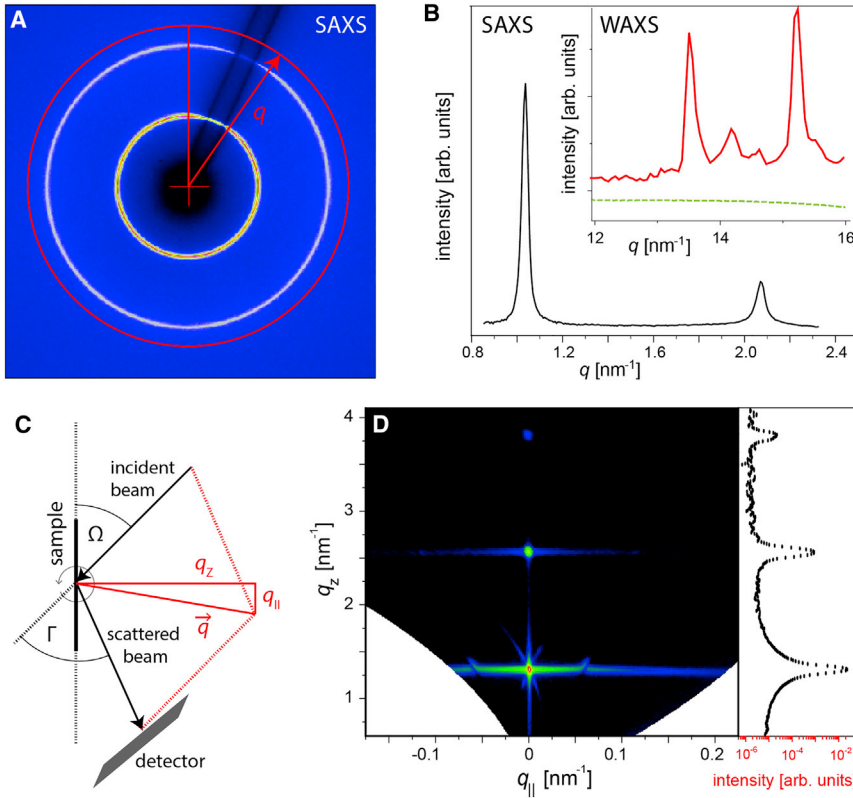
FIGURE 2 Small-angle x-ray scattering (SAXS) and neutron diffraction (ND) experiments. (*A*) A representative 2D SAXS pattern featuring first- and second-order Bragg peaks in the form of concentric rings is shown. (*B*) A radial plot of the integration in the azimuthal direction of SAXS pattern with first- and second-order Bragg peaks is shown. Inset: WAXS region exhibiting peaks only for exceptional samples in the chain-ordered L_β phase (here: *Psyc-sat; f_{gly} = 1.0; 50°C; solid red curve*). For typical samples in the fluid L_α phase (here: *LacCer-sat; f_{gly} = 0.1 in DMPC; 50°C; dashed green curve*), no WAXS peaks are observed. (*C*) A schematic illustration of the experimental geometry for ND in top view is shown. (*D*) A typical ND reciprocal space map, $S(q_z, q_{||})$, featuring three Bragg sheet orders (here: *DGDG-sat; f_{gly} = 0.5 in DMPC; 50°C, h_{rel} = 95%*), is shown. Plot on the right: specular intensity ($q_{||} \approx 0$) as a function of q_z. To see this figure in color, go online.

Fig. 2 *B*, additional peaks in the wide-angle region (at $q \approx 15$ nm^{-1}) occur for membranes in the chain-ordered L_β phase (30). Conversely, the absence of these peaks in most of the measurements confirms that the membranes investigated are in the fluid L_α phase.

ND

ND measurements with solid-supported membrane multilayers were performed on the high-resolution diffractometer D16 at Institut Laue-Langevin (ILL, Grenoble, France). Fig. 2 *C* shows the geometry of the experiment in a view from the top. The incident beam with a wavelength of $\lambda = 0.4518$ nm hits the sample plane with an adjustable angle of incidence Ω and is scattered into various directions at angles Γ with respect to the incident beam. For each Ω, the Γ-dependent intensity is recorded with a position-sensitive ^{3}He detector (MILAND, ILL) with a distance of 950 mm to the sample. By rotating the sample stage, and thus by stepwise variation of Ω, two-dimensional maps of the intensity as a function of Γ and Ω are recorded. During this procedure, the intensity is normalized to the intensity of the incident beam (via an in-beam monitor), the detector channel sensitivity, and the illuminated sample area. Further details of the ND measurements are reported elsewhere (19). The angles Γ and Ω are associated with the reciprocal space coordinates q_z and $q_{||}$, i.e., the scattering vector components perpendicular and parallel to the sample plane, respectively, according to the geometrical relations $q_z = (2\pi/\lambda)[\sin(\Gamma - \Omega) + \sin(\Omega)]$ and $q_{||} = (2\pi/\lambda)[\cos(\Gamma - \Omega) - \cos(\Omega)]$; see Fig. 2 *C*. The main panel of Fig. 2 *D* shows a typical reciprocal space map, i.e., a map of the intensity as a function of q_z and $q_{||}$, termed $S(q_z, q_{||})$ in the following. It features the characteristic horizontal "Bragg sheets" of planar membrane multilayers (31). Whereas the scattering intensity along the specular line ($\Gamma = 2\Omega$, $q_{||} = 0$; see Fig. 2 *D*, *right*) contains information on the structure perpendicular to the surface (notably the lamellar periodicity as encoded in the Bragg peak positions and the scattering length density profile as encoded in the peak intensities), the diffuse scattering intensity ($\Gamma \neq 2\Omega$,

$q_{||} \neq 0$) along the Bragg sheets additionally contains information on the in-plane structure, notably the membrane fluctuations in terms of their spatial self- and cross-correlation functions. Within the framework of a discrete smectic Hamiltonian of interacting multilayers, these correlation functions are in turn governed by the mechanical properties of the interacting membranes in terms of the membrane bending modulus κ and the intermembrane compression modulus B (32). As we have shown earlier, the experimentally obtained reciprocal space maps within this framework can be satisfactorily modeled solely based on the underlying mechanical parameters κ and B and on an empirical cutoff parameter termed R (8,19,33). In practice, this procedure relies on the kinematic approximation (KA) of wave scattering because application of the more accurate distorted-wave Born approximation (34) would require detailed additional knowledge of the sample structure, which is unavailable. As a consequence, our KA-based treatment, which is only valid wherever the intensity is weak compared to the incident beam, does not correctly capture the specular maximum of the first Bragg sheet, where this condition is typically violated. Although in the past, we therefore ignored the first Bragg sheet and relied on the second one (8,19,33), we here combine information from the first two Bragg sheets (see Fig. 4): whereas the Caillé parameter

$$\eta = \pi k_B T \Big/ \left(2d^2 \sqrt{\kappa B/d} \right) \tag{1}$$

is obtained from the specular/diffuse scattering intensity ratio in the second Bragg sheet, the de Gennes parameter

$$\Lambda = \sqrt{\kappa/(Bd)} \tag{2}$$

is obtained from the decay of the off-specular intensity in the first Bragg sheet along $q_{||}$, excluding the specular intensity that violates the KA. The best matching values of η, Λ, and R are then determined by their systematic
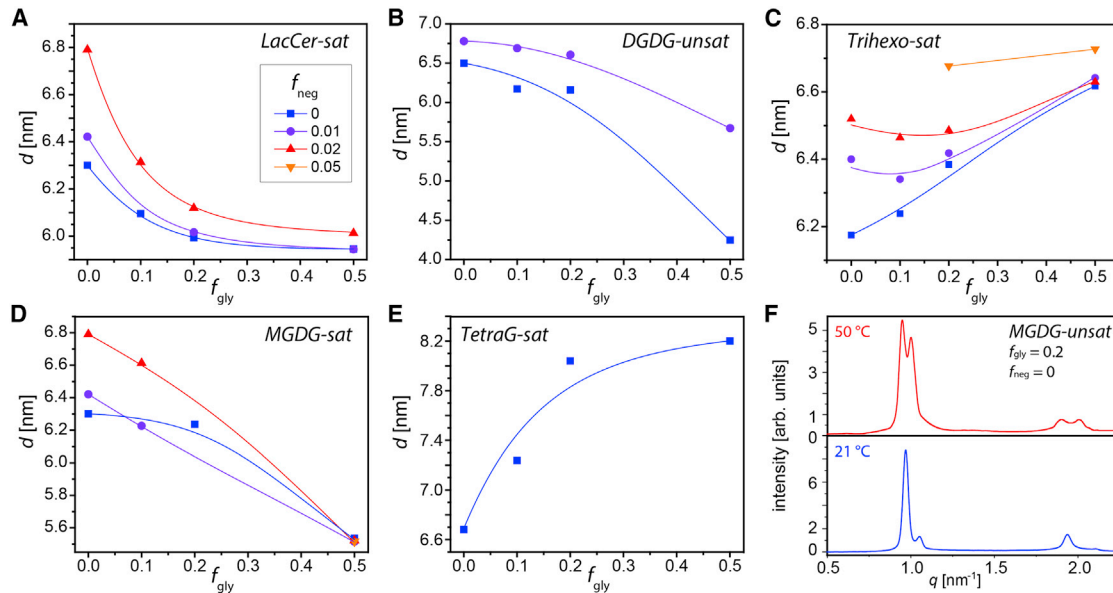
FIGURE 3 Lamellar periodicities d obtained by SAXS for of PC lipid membrane multilayers containing different fractions f_{gly} of glycolipids and f_{neg} of negatively charged lipids. (A) *LacCer-sat*, (B) *DGDG-unsat*, (C) *Trihexo-sat*, (D) *MGDG-sat*, and (E) *TetraG-sat* are shown. Solid lines are guides to the eye. The measurements were conducted at 21°C (B) or 50°C (A, C, D, and E). (F) Radial plots of the integration in the azimuthal direction of the SAXS patterns of PC lipid membranes containing MGDG-unsat ($f_{gly} = 0.2, f_{neg} = 0$) at 21°C (*bottom*) and 50°C (*top*) are shown. To see this figure in color, go online.

variation in the model until the best agreement with the experimental data is achieved. Finally, the mechanical parameters are obtained by solving Eqs. 1 and 2 for κ and B.

ND measurements were conducted above the matrix lipid phase transition temperature (Table 1), either at 30°C (for samples based on POPC) or 50°C (for samples based on DMPC or DPPC). For measurements at controlled osmotic pressure, the beamline humidity chamber was used (35), providing simultaneous control of temperature and relative humidity (h_{rel}). The corresponding osmotic pressure is given as

$$\Pi = \frac{k_B T}{v_w} ln(h_{rel}), \qquad (3)$$

where $v_w = 0.03$ nm^3 denotes the molecular volume of water, and k_B is the Boltzmann constant. For measurements under bulk water conditions, a "sandwich" cell composed of two parallel chips was used (33). To achieve optimal scattering length density contrast, the samples were measured with D$_2$O vapor or in D$_2$O-based buffers.

RESULTS AND DISCUSSION

Fig. 1 A schematically illustrates self-assembled multilayers of lipid membranes interacting in an aqueous environment. The membranes are composed of up to three lipid components with molar fractions f, where $f = 1$ corresponds to 100 mol%. PC lipids POPC, DMPC, and DPPC are used as the matrix, with the mole fraction $f_{PC} = 1 - f_{gly} - f_{neg}$ accommodating glycolipids (see Fig. 1 B) with the mole fraction $f_{gly} \, \varepsilon \, \{0, 0.1, 0.2, 0.5\}$ and negatively charged lipids (with phosphatidylserine or phosphatidylglycerol headgroups) with the mole fraction $f_{neg} \, \varepsilon \, \{0, 0.01, 0.02, 0.05\}$. The negatively charged lipids are introduced to exert defined repulsive electrostatic forces between neighboring membranes (see further below). For each glycolipid species, the PC lipid and negatively charged lipid species were
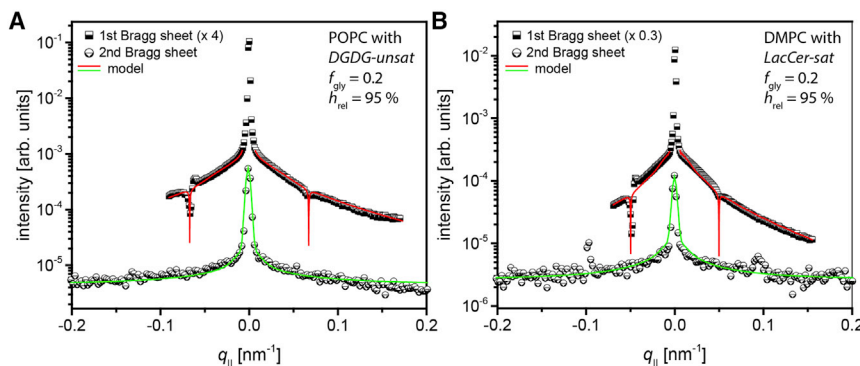

FIGURE 4 Intensities of the first and second Bragg sheets of (A) POPC membranes loaded with *DGDG-unsat* at $f_{gly} = 0.2$ and $f_{neg} = 0$ and (B) DMPC membranes loaded with *LacCer-sat* at $f_{gly} = 0.2$ and $f_{neg} = 0$, both at $h_{rel} = 95\%$. Solid lines: simulated intensities corresponding to the best matching parameters η and Λ in the continuum-mechanical model (see main text). To see this figure in color, go online.

chosen to match the alkyl chain length of the glycolipid and the respective number and position of double bonds in the chain (see Table 2) to assure the miscibility of all three lipid components.

The configuration illustrated in Fig. 1 A equally applies to the multilayered membrane aggregates investigated by SAXS/WAXS and to the solid-supported aligned multilayers investigated by ND. The separation between the surfaces of neighboring membranes (i.e., the water layer thickness d_w) is encoded in the lamellar period d of the multilayers according to $d = d_m + d_w$, where d_m denotes the membrane thickness.

The plots in Fig. 3 show d as a function of the glycolipid mole fraction for selected glycolipid types. The values of d are obtained from the q-positions of the Bragg peaks, as $d = 2n\pi/q_{peak}$, where n (= 1, 2, …) is the order of the peak (see Materials and Methods). It should be noted that the lipid membranes are in the biologically relevant fluid L_α phase, indicated by the absence of a chain-ordering peak in the WAXS region (30) (see Fig. 2 B). When neglecting variations in the membrane thickness, a reduction in d upon addition of glycolipids indicates that the contribution of the glycolipids to the membrane interaction is attractive, whereas an increase indicates a repulsive contribution. Similarly, the observed increase in d upon addition of negatively charged lipids reflects their repulsive electrostatic contribution to the membrane interaction. For weakly charged surfaces in a monovalent electrolyte, the pressure Π_{el} associated with the electrostatic repulsion is given as (36)

TABLE 2 Investigated Glycolipids Together with the Corresponding Matrix Lipids and Negatively Charged Lipids If Applicable

Glycolipid	Abbreviation	Matrix Lipid	Negatively Charged Lipid
N-hexadecanoyl lactosyl-ceramide	*LacCer-sat*	DMPC	DMPG
N-Pentadecanoyl psychosine	*Psyc-sat*	DMPC	DMPG
Monogalactosyl-diacylglycerol saturated	*MGDG-sat*	DMPC	DMPG
Monogalactosyl-diacylglycerol unsaturated	*MGDG-unsat*	POPC	POPS
Digalactosyl-diacylglycerol saturated	*DGDG-sat*	DMPC	DMPG
Digalactosyl-diacylglycerol unsaturated	*DGDG-unsat*	POPC	POPS
N-hexadecanoyl-ceramide trishexoside	*Trihexo-sat*	DMPC	DMPG
Gangliotetraosyl-ceramide	*TetraG-sat*	DPPC	DPPG

$$\Pi_{el}(d_w) \cong 2k_BT\rho_0[\cosh(e\psi_m(d_w)/k_BT) - 1], \quad (4)$$

where ρ_0 is the number density of monovalent ions according to their bulk concentration of $c_0 = 100$ mM, e is the electron charge, and ψ_m is the electric potential at the midplane (i.e., the center of the water layer), which depends on the charge density of the surfaces (see Supporting Materials and Methods) and is thus determined by f_{neg}. Note that the strength of the repulsion may be affected in general by charge regulation when the charged groups are protonatable (37). The repulsion associated with the incorporation of negatively charged lipids is seen most prominently for interacting PC membranes without glycolipids ($f_{gly} = 0$; see Fig. 3), for which d, and thus the membrane separation d_w, considerably increases with increasing f_{neg}. The extent of this increase is governed by a subtle balance of interfacial forces acting between the membranes, namely van der Waals attraction on one side versus hydration repulsion (9,38), undulation repulsion, and electrostatic repulsion on the other side (16). For DMPC bilayers with $f_{neg} = 0.02$ in 100 mM monovalent salt at $d = 6.3$ nm (see Fig. 3 A), $d_w = 2.8$ nm (as follows from $d_m = 3.5$ nm (39)), and Eq. 4 yields $\Pi_{el} \approx 4 \times 10^3$ Pa, comparable to the hydration repulsion and the van der Waals attraction at the same separation, both on the order of 10^3–10^4 Pa (40). It should be noted that when introducing charged lipids, one strictly does not only introduce charge but may also induce other changes, albeit the former can be considered to be the dominant effect. Varying the electrostatic repulsion alternatively by variation of the salt concentration must be considered problematic because ions can influence the saccharide binding (41,42) and lead to effective surface charges due to preferential interactions with PC lipids (19,43) or glycolipids (44).

In the following, the influence of the glycolipid type and mole fraction on the interaction of PC lipid membranes is discussed. Fig. 3 A shows $d(f_{gly})$ for DMPC membranes loaded with *LacCer-sat*, a glycolipid with a disaccharide headgroup (see Fig. 1 B). In the absence of negatively charged lipids ($f_{neg} = 0$), d assumes a value of ≈ 6.3 nm at $f_{gly} = 0$, in agreement with the literature (39). It decreases as a function of f_{gly} until it saturates at $d \approx 6.0$ nm, a value that appears to be governed by this particular glycolipid. The f_{gly} dependence of d is clearly nonlinear: already low *LacCer-sat* fractions ($f_{gly} = 0.1$) lead to a considerable reduction in d, which suggests that the glycolipids are able to pull the membranes closer together. Even more strikingly, the impact of negatively charged lipids (DMPG) on d diminishes systematically with increasing f_{gly}. Whereas the pure phospholipid membranes ($f_{gly} = 0$) exhibit a response of as much as $\Delta d \approx 0.5$ nm to the incorporation of 2 mol% negatively charged lipids ($f_{neg} = 0.02$), a much weaker response to the same level of electrostatic repulsion is observed when the membranes contain *LacCer-sat* ($\Delta d \approx$ 0.15 nm at $f_{gly} = 0.2$; $\Delta d \approx 0.08$ nm at $f_{gly} = 0.5$). This

result is very similar to what was reported earlier for the special *LewisX* trisaccharide motif (19) and clearly indicates that *LacCer-sat* glycolipids with disaccharide headgroups hold the membranes together, even against electrostatic repulsion. The remaining variability in d even under cross-linked conditions reflects that the lipid tails anchoring the saccharides into the bilayers are not entirely rigid but can be partially pulled out of the bilayers when subject to tensile forces. Moreover, the binding between two saccharides itself must be considered "diffuse," meaning that it can involve a number of different configurations with different "bond lengths" (45). In contrast, for a glycolipid with a different disaccharide headgroup (*DGDG-unsat* incorporated in a POPC matrix; see Fig. 3 *B*), there is no indication of such membrane cross-linking. Instead of already observing a strong response of the periodicity at low f_{gly} followed by a saturation, pronounced changes only occur for high f_{gly} and without any indication of saturation. Moreover, the effect of negative charges remains pronounced even at high f_{gly}, in contrast to the case of *LacCer-sat*. The simplest explanation for this qualitatively different behavior is that the digalactose headgroups of *DGDG-unsat* have a much weaker tendency to be engaged in homotypic intermembrane "binding" than the lactose headgroups of *LacCer-sat*. Fig. 3 *C* shows $d(f_{gly})$ for DMPC membranes loaded with *Trihexo-sat*, a glycolipid with a trisaccharide headgroup (see Fig. 1 *B*). The overall behavior is similar to that of *LacCer-sat*, but the value at which d saturates for high f_{gly} ($d \approx 6.6$ nm), i.e., the membrane separation preferred by this saccharide headgroup is larger than that of the pure PC membranes ($d \approx 6.2$ nm), which can be attributed to the bulkier trisaccharide headgroups. As in case of *LacCer-sat*, d becomes rather insensitive to electrostatic repulsion for sufficiently high glycolipid fractions. In fact, for $f_{gly} \geq 0.2$, the adjacent membranes are still stably cross-linked by *Trihexo-sat* even at comparatively high fractions of negatively charged DMPG lipids ($f_{neg} = 0.05$), whereas for $f_{gly} \leq 0.1$, the multilamellar architecture is not stable against the considerable electrostatic repulsion, and no lamellar periodicity can be specified. When comparing the chemistries of *LacCer-sat* and *Trihexo-sat* (which are both found to hold membranes together) with that of *DGDG-unsat* (which does not hold membranes together), one apparent difference is that the former two comprise a lactose motif, whereas the latter does not. This correlation may suggest that lactose strongly contributes to preferential interactions favoring homotypic saccharide contacts. In fact, lactose is much less water soluble (≈ 19 g/dL) than other abundant disaccharides (46–48) such as sucrose (≈ 200 g/dL), maltose (≈ 110 g/dL), or trehalose (~ 70 g/dL), reflecting favorable lactose-lactose interactions in water, in line with the above hypothesis.

Coming back to Fig. 3 *D* shows $d(f_{gly})$ for DMPC membranes loaded with *MGDG-sat*, a glycolipid with a monogalactose headgroup (see Fig. 1 *B*). Independent of the fraction of negatively charged lipids (DMPG), d decreases with increasing f_{gly} until it reaches a value of $d \approx 5.5$ nm at $f_{gly} = 0.5$. As in case of *DGDG-unsat*, the decrease is approximately linear with f_{gly} and does not exhibit any tendency of saturation. However, in contrast to *DGDG-unsat*, d for *MGDG-sat* is less sensitive to electrostatic repulsion for high f_{gly}. This may indicate that the monogalactose headgroups of *MGDG-sat* in principle have the tendency to engage into homotypic membrane binding but are sterically hindered for low f_{gly} because they are "buried" within the PC headgroup layer because of their compactness. This interpretation is corroborated by the observation that also other glycolipids with monosaccharide headgroups are unable to cross-link PC lipid membranes at low f_{gly} (for example, *Psyc-sat*; see Supporting Materials and Methods). Fig. 3 *E* shows $d(f_{gly})$ for DPPC membranes loaded with *TetraG-sat*, a glycolipid with a linear tetrasaccharide headgroup (see Fig. 1 *B*). It is seen that d strongly increases with f_{gly}, rapidly at first until it saturates at $d \approx 8.1$ nm. For these glycolipids with their comparatively bulky headgroups, steric repulsion appears to be dominating the membranes' equilibrium separation, whereas the influence of electrostatic repulsion via incorporation of negatively charged lipids ($f_{neg} \neq 0$) is insignificant (see Supporting Materials and Methods). The f_{gly} dependence of d is reminiscent of that of DPPC membranes loaded with *LewisX* lipids, whose headgroups are of similar bulkiness (19).

Finally, it should be noted that incorporation of glycolipids into PC lipid membranes can also affect the lamellar periodicity d in an indirect way via their influence on the membrane thickness d_m (see Fig. 1 *A*). This effect, which can be assumed to be approximately linear in f_{gly}, does not, however, impede the conclusions drawn here because it does not affect the response of d to electrostatic repulsion.

As exemplified in Fig. 3 *F* for *MGDG-unsat* at $f_{gly} = 0.2$ and $f_{neg} = 0$, significant splitting of the SAXS Bragg peaks is observed in certain cases, indicating that phase separation into membrane multilayers with different lamellar periodicities occurs. This phase separation can be attributed to conflicting membrane separations preferred by the attraction-inducing membrane components (the glycolipids) and the more repulsive membrane components (the phospholipids). Interestingly, the separation is found predominantly for glycolipids with monosaccharide headgroups (*MGDG* and *Psyc*), which are unable to establish direct inter-bilayer contacts under monophasic conditions in which they do not protrude from the headgroup layer of the PC lipid matrix (see above). This behavior is observed at a low temperature (21°C, Fig. 3 *F*, *bottom*) and at high temperature (50°C, Fig. 3 *F*, *top*). It is closely related to the results of earlier microscopy studies on solid-supported lipid membranes comprising lipopolymers inducing steric repulsion and biotin lipids inducing strong binding via streptavidin, in which the adhesion was found to be accompanied by lateral phase separation featuring domains of tight adhesion

(49,50). More recently, the adhesion of multicomponent membranes containing attraction-inducing and repulsion-inducing components was also studied theoretically (51). In that work, it was shown that the segregation pattern depends on the strength of the repulsive component which opposes binding. In view of these experimental and theoretical reports, we conclude that the observed phase separation constitutes additional evidence for the glycolipids' tendency to induce attraction between neighboring lipid membranes. Coming back to the SAXS data in Fig. 3 F, the coexistence of two sets of Bragg peaks indicates that the different phases are aligned in registry in the multilayers. As proposed by Kollmitzer et al. (52), such behavior can result from the different strengths of hydration (14) and undulation forces in the glycolipid-rich and phospholipid-rich phases.

To explore to what extent the glycolipids' cross-linking abilities identified here by SAXS have their manifestation also with regard to the mechanical properties of interacting membranes, ND on solid-supported membrane multilayers was carried out. In an earlier study (19), such measurements revealed a considerable influence of the density of *LewisX* lipids (see Introduction) on the intermembrane compression modulus B (see ND), reflecting a rigidification through the formation of saccharide bonds. Fig. 4 shows the first two Bragg sheets recorded by ND with a system unable to form bonds (POPC membranes loaded with *DGDG-unsat* at $f_{\mathrm{gly}} = 0.2$ and $f_{\mathrm{neg}} = 0$; Fig. 4 A) and with a system able to form bonds (DMPC membranes loaded with *LacCer-sat* at $f_{\mathrm{gly}} = 0.2$ and $f_{\mathrm{neg}} = 0$; Fig. 4 B). Plotted are the q_z-integrated Bragg sheet intensities (in practice, the integration is performed in the Γ direction (8,19,33)) as functions of $q_{\parallel}$, featuring the respective central specular maxima symmetrically flanked by the slowly decaying diffuse scattering intensity. The latter is locally decorated with minima at conditions of high absorption ($\Omega \approx 0$ and $\Omega \approx \Gamma$) and peaks arising from multiple scattering effects (19). Both data sets are from measurements at $h_{\mathrm{rel}} = 95\%$ (corresponding to a moderate dehydrating osmotic pressure of $\Pi \approx 8 \times 10^6$ Pa; see Eq. 3) and not from measurements under bulk water conditions, in which the intensities of the second Bragg sheets were found to be too weak to be analyzed (see Supporting Materials and Methods). The reason for these low intensities is a minimum in the membrane form factor, which essentially coincides with the position of second Bragg sheets because of the near-identical thicknesses of the hydrogenous region (the alkyl chain layer) and the deuterated region (the hydrated headgroup

layer). In fact, even under the slightly dehydrated conditions shown in Fig. 4, the information contained in the second Bragg sheets (primarily on the Caillé parameter, η) needed to be complemented with that of the first Bragg sheets (on the de Gennes parameter, Λ), as described in the section "ND." The solid lines superimposed to the experimental data points represent simulated Bragg sheet intensities corresponding to the best matching parameters η and Λ in the continuum-mechanical model simultaneously describing the first and second Bragg sheets. Absorption close to $\Omega \approx 0$ and $\Omega \approx \Gamma$ was modeled as described in the Supporting Materials and Methods.

The best matching model parameters for both systems are summarized in Table 3, together with the mechanical parameters κ and B derived thereof according to Eqs. 1 and 2. For the membranes containing *DGDG-unsat* (unable to form saccharide bonds; see Fig. 3 B), as well as for the membranes containing *LacCer-sat* (able to form saccharide bonds; see Fig. 3 A), the obtained bending rigidities κ fall into the range of $\approx 10^{-19}$ J (or ≈ 25 k_BT), consistent with earlier reports on membranes in the fluid L_α phase (8,19,53,54) and with the observation that κ is rather insensitive to the hydration level (8,54). The similarity of the values obtained here with those reported earlier for glycolipid-free PC lipid membranes indicates that the saccharide headgroups at a lateral concentration of $f_{\mathrm{gly}} = 0.2$ do not influence the bending rigidity much, in line with our earlier work on *LewisX* lipids (19). Moving on to the compression moduli B in Table 3, we notice that their values differ considerably between the two investigated membrane systems. Surprisingly, the value is higher for the system unable to form saccharide bonds, in contrast to our earlier finding that B increases with increasing bond density, at least under bulk water conditions (19). This discrepancy suggests that under conditions of partial dehydration, direct steric repulsion between the membrane surfaces rather than the bonds may be the dominant contribution to the compression modulus. Indeed, the moduli obtained here ($B \geq 3$ MPa) are much higher than those obtained previously under bulk water conditions (<1 MPa), in which the bonds were found to be the dominant contribution (19). Based on this notion, we conclude that ND on membrane multilayers in general is a promising approach to quantify the effect of saccharide binding on membrane mechanical properties, in particular when information from two Bragg sheets is exploited as introduced here. However, the detailed analysis of mechanical parameters under bulk water conditions requires

TABLE 3 Best Matching Parameters, as Obtained by ND, of Selected Membrane Multilayer Systems Containing Glycolipids

Sample: *Glycolipid*/Phospholipid	h_{rel}	T [°C]	η	Λ [Å]	R [µm] for First BS/Second BS	κ [J]	κ [k_BT]	B [MPa]
DGDG-unsat/POPC, $f_{\mathrm{gly}} = 0.2$; $f_{\mathrm{neg}} = 0$	95%	30	0.015	12	2.5/1.2	1.1×10^{-19}	27	16
LacCer-sat/DMPC, $f_{\mathrm{gly}} = 0.2$; $f_{\mathrm{neg}} = 0$	95%	50	0.029	25	1.1/1.1	1.1×10^{-19}	25	3

Caillé parameter, η; De Gennes parameter, Λ; cutoff radius, R, for the first two BSs; membrane bending modulus, κ; intermembrane compression modulus, B (see Materials and Methods for definitions). BS, Bragg sheet.

avoiding unfavorably placed form factor minima. In the future, this can be achieved by the use of chain-deuterated (matrix) lipids in combination with light water (H_2O) or by the use of lipids with significantly longer or shorter tails.

CONCLUSIONS

With the help of x-ray and neutron scattering techniques, we have studied the influence of various commercially available glycolipids on the interaction between adjacent phospholipid bilayers to test whether or not the glycolipids promote membrane adhesion via the formation of saccharide bonds. Some of the saccharide headgroup types investigated were found to be able to bind adjacent membranes together, even against the repulsive forces generated by introducing defined fractions of negatively charged phospholipids. This finding indicates that glycolipid-mediated membrane adhesion is potentially highly abundant in biology and therefore merits further investigation, in particular with regard to its biological role. In this work, the cross-linking ability of glycolipids was not found to have any significant influence on the membrane bending rigidity. In certain cases, headgroup-driven phase separation into membrane multilayers with different lamellar periodicities occurs because of the conflicting membrane separations preferred by the glycolipids and the phospholipids.

SUPPORTING MATERIAL

Supporting Material can be found online at https://doi.org/10.1016/j.bpj.2020.02.003.

AUTHOR CONTRIBUTIONS

V.M.L. and E.S. designed the research. V.M.L., B.D., and E.S. performed experiments. B.D. contributed analytic tools. V.M.L., B.D., and E.S. analyzed the data. V.M.L. and E.S. wrote the manuscript.

ACKNOWLEDGMENTS

SUPPORTING CITATIONS

Reference (55) can be found in the Supporting Material.

REFERENCES

1. Alberts, B., A. Johnson, …, P. Walter. 1983. Molecular Biology of the Cell. Garland Science, New York.

2. Schneck, E. 2017. The interaction between soft interfaces: forces and structural aspects. *Advanced Materials Interfaces.* 4:1600349.

3. Stoffel, W., and A. Bosio. 1997. Myelin glycolipids and their functions. *Curr. Opin. Neurobiol.* 7:654–661.

4. Boudière, L., M. Michaud, …, E. Maréchal. 2014. Glycerolipids in photosynthesis: composition, synthesis and trafficking. *Biochim. Biophys. Acta.* 1837:470–480.

5. Ryrie, I. J., J. M. Anderson, and D. J. Goodchild. 1980. The role of the light-harvesting chlorophyll a/b protein complex in chloroplast membrane stacking. Cation-induced aggregation of reconstituted proteoliposomes. *Eur. J. Biochem.* 107:345–354.

6. Webb, M. S., and B. R. Green. 1990. Effects of neutral and anionic lipids on digalactosyldiacylglycerol vesicle aggregation. *Biochim. Biophys. Acta.* 1030:231–237.

7. Demé, B., C. Cataye, …, J. Jouhet. 2014. Contribution of galactoglycerolipids to the 3-dimensional architecture of thylakoids. *FASEB J.* 28:3373–3383.

8. Schneck, E., F. Rehfeldt, …, M. Tanaka. 2008. Modulation of intermembrane interaction and bending rigidity of biomembrane models via carbohydrates investigated by specular and off-specular neutron scattering. *Phys. Rev. E Stat. Nonlin. Soft Matter Phys.* 78:061924.

9. Parsegian, V. A., N. Fuller, and R. P. Rand. 1979. Measured work of deformation and repulsion of lecithin bilayers. *Proc. Natl. Acad. Sci. USA.* 76:2750–2754.

10. Marra, J. 1985. Controlled deposition of lipid monolayers and bilayers onto mica and direct force measurements between galactolipid bilayers in aqueous solutions. *J. Colloid Interface Sci.* 107:446–458.

11. Marra, J. 1986. Direct measurements of attractive Van der Waals and adhesion forces between uncharged lipid bilayers in aqueous solutions. *J. Colloid Interface Sci.* 109:11–20.

12. Ricoul, F., M. Dubois, …, I. Rico-Lattes. 1998. Phase equilibria and equation of state of a mixed cationic Surfactant−Glycolipid lamellar system. *Langmuir.* 14:2645–2655.

13. Wood, J., P. Luckham, and R. Swart. 1993. Exploring the interactions between glycolipid bilayers. *Colloids Surf. A Physicochem. Eng. Asp.* 77:179–189.

14. Kanduč, M., A. Schlaich, …, E. Schneck. 2017. Tight cohesion between glycolipid membranes results from balanced water-headgroup interactions. *Nat. Commun.* 8:14899.

15. Leontidis, E., A. Aroti, …, T. Zemb. 2007. Effects of monovalent anions of the hofmeister series on DPPC lipid bilayers Part II: modeling the perpendicular and lateral equation-of-state. *Biophys. J.* 93:1591–1607.

16. Schlaich, A., B. Kowalik, …, R. R. Netz. 2015. Physical mechanisms of the interaction between lipid membranes in the aqueous environment. *Physica A.* 418:105–125.

17. Gourier, C., F. Pincet, …, P. Sinaÿ. 2004. Specific and non specific interactions involving LeX determinant quantified by lipid vesicle micromanipulation. *Glycoconj. J.* 21:165–174.

18. Eggens, I., B. Fenderson, …, S. Hakamori. 1989. Specific interaction between Lex and Lex determinants. A possible basis for cell recognition in preimplantation embryos and in embryonal carcinoma cells. *J. Biol. Chem.* 264:9476–9484.

19. Schneck, E., B. Demé, …, M. Tanaka. 2011. Membrane adhesion via homophilic saccharide-saccharide interactions investigated by neutron scattering. *Biophys. J.* 100:2151–2159.

20. Yu, Z. W., T. L. Calvert, and D. Leckband. 1998. Molecular forces between membranes displaying neutral glycosphingolipids: evidence for carbohydrate attraction. *Biochemistry.* 37:1540–1550.

21. Chatterjee, S. 1991. Lactosylceramide stimulates aortic smooth muscle cell proliferation. *Biochem. Biophys. Res. Commun.* 181:554–561.

22. Li, X.-M., M. M. Momsen, ..., R. E. Brown. 2002. Lactosylceramide: effect of acyl chain structure on phase behavior and molecular packing. *Biophys. J.* 83:1535–1546.

23. Sonnino, S., A. Prinetti, ..., K. Iwabuchi. 2009. Role of very long fatty acid-containing glycosphingolipids in membrane organization and cell signaling: the model of lactosylceramide in neutrophils. *Glycoconj. J.* 26:615–621.

24. Ashkenazi, S., and T. G. Cleary. 1989. Rapid method to detect shiga toxin and shiga-like toxin I based on binding to globotriosyl ceramide (Gb3), their natural receptor. *J. Clin. Microbiol.* 27:1145–1150.

25. Saiman, L., and A. Prince. 1993. *Pseudomonas aeruginosa* pili bind to asialoGM1 which is increased on the surface of cystic fibrosis epithelial cells. *J. Clin. Invest.* 92:1875–1880.

26. Rondelli, V., P. Brocca, ..., E. Del Favero. 2017. Membrane restructuring following in situ sialidase digestion of gangliosides: complex model bilayers by synchrotron radiation reflectivity. *Biochim Biophys Acta Biomembr.* 1859:845–851.

27. Rockland, L. B. 1960. Saturated salt solutions for static control of relative humidity between 5° and 40° C. *Anal. Chem.* 32:1375–1376.

28. Paris, O., C. Li, ..., P. Fratzl. 2007. A new experimental station for simultaneous X-ray microbeam scanning for small- and wide-angle scattering and fluorescence at BESSY II. *J. Appl. Cryst.* 40:s466–s470.

29. Benecke, G., W. Wagermaier, ..., P. Fratzl. 2014. A customizable software for fast reduction and analysis of large X-ray scattering data sets: applications of the new *DPDAK* package to small-angle X-ray scattering and grazing-incidence small-angle X-ray scattering. *J. Appl. Cryst.* 47:1797–1803.

30. Mills, T. T., J. Huang, ..., J. F. Nagle. 2009. Effects of cholesterol and unsaturated DOPC lipid on chain packing of saturated gel-phase DPPC bilayers. *Gen. Physiol. Biophys.* 28:126–139.

31. Salditt, T. 2005. Thermal fluctuations and stability of solid-supported lipid membranes. *J. Phys. Condens. Matter.* 17:R287–R314.

32. Lei, N., C. R. Safinya, and R. F. Bruinsma. 1995. Discrete harmonic model for stacked membranes: theory and experiment. *J. Phys. II France.* 5:1155–1163.

33. Schneck, E., R. G. Oliveira, ..., M. Tanaka. 2009. Mechanical properties of interacting lipopolysaccharide membranes from bacteria mutants studied by specular and off-specular neutron scattering. *Phys. Rev. E Stat. Nonlin. Soft Matter Phys.* 80:041929.

34. Sinha, S. K., E. B. Sirota, ..., H. B. Stanley. 1988. X-ray and neutron scattering from rough surfaces. *Phys. Rev. B Condens. Matter.* 38:2297–2311.

35. Gonthier, J., M. A. Barrett, ..., E. Lelièvre-Berna. 2019. BerILL: the ultimate humidity chamber for neutron scattering. *J. Neutron Res.* 21:65–76.

36. Israelachvili, J. N. 2011. Intermolecular and Surface Forces. Academic Press, Waltham, MA.

37. Majee, A., M. Bier, ..., R. Podgornik. 2019. Charge regulation radically modifies electrostatics in membrane stacks. *Phys. Rev. E.* 100:050601.

38. Schneck, E., F. Sedlmeier, and R. R. Netz. 2012. Hydration repulsion between biomembranes results from an interplay of dehydration and depolarization. *Proc. Natl. Acad. Sci. USA.* 109:14405–14409.

39. Lis, L. J., M. McAlister, ..., V. A. Parsegian. 1982. Interactions between neutral phospholipid bilayer membranes. *Biophys. J.* 37:657–665.

40. Demé, B., M. Dubois, and T. Zemb. 2002. Swelling of a lecithin lamellar phase induced by small carbohydrate solutes. *Biophys. J.* 82:215–225.

41. Geyer, A., C. Gege, and R. R. Schmidt. 1999. Carbohydrate-carbohydrate recognition between LewisX glycoconjugates. *Angew. Chem. Int.Engl.* 38:1466–1468.

42. Nodet, G., L. Poggi, ..., G. Bodenhausen. 2007. Weak calcium-mediated interactions between Lewis X-related trisaccharides studied by NMR measurements of residual dipolar couplings. *J. Am. Chem. Soc.* 129:9080–9085.

43. Lotan, O., L. Fink, ..., U. Raviv. 2016. Critical conditions for adsorption of calcium ions onto dipolar lipid membranes. *J. Phys. Chem. A.* 120:3390–3396.

44. Stefaniu, C., V. M. Latza, ..., E. Schneck. 2019. Headgroup-ordered monolayers of uncharged glycolipids exhibit selective interactions with ions. *J. Phys. Chem. Lett.* 10:1684–1690.

45. Kav, B. 2019. Membrane adhesion mediated via lipid-anchored saccharides. PhD thesis. University of Potsdam.

46. Higashiyama, T. 2002. Novel functions and applications of trehalose. *Pure Appl. Chem.* 74:1263–1269.

47. Machado, J. J. B., J. A. Coutinho, and E. A. Macedo. 2000. Solid-liquid equilibrium of alpha-lactose in ethanol/water. *Fluid Phase Equilib.* 173:121–134.

48. Mathlouthi, M., and P. Reiser. 2012. Sucrose: Properties and Applications. Springer Science & Business Media, Dordrecht.

49. Albersdörfer, A., T. Feder, and E. Sackmann. 1997. Adhesion-induced domain formation by interplay of long-range repulsion and short-range attraction force: a model membrane study. *Biophys. J.* 73:245–257.

50. Kloboucek, A., A. Behrisch, ..., E. Sackmann. 1999. Adhesion-induced receptor segregation and adhesion plaque formation: a model membrane study. *Biophys. J.* 77:2311–2328.

51. Weikl, T. R., J. T. Groves, and R. Lipowsky. 2002. Pattern formation during adhesion of multicomponent membranes. *EPL.* 59:916–922.

52. Kollmitzer, B., P. Heftberger, ..., G. Pabst. 2015. Bending rigidities and interdomain forces in membranes with coexisting lipid domains. *Biophys. J.* 108:2833–2842.

53. Dimova, R. 2014. Recent developments in the field of bending rigidity measurements on membranes. *Adv. Colloid Interface Sci.* 208:225–234.

54. Pan, J., S. Tristram-Nagle, ..., J. F. Nagle. 2008. Temperature dependence of structure, bending rigidity, and bilayer interactions of dioleoylphosphatidylcholine bilayers. *Biophys. J.* 94:117–124.

55. National Institute of Standards and Technology 2013. NIST Center for Neutron Research Neutron Activation and Scattering Calculator https://www.ncnr.nist.gov/resources/activation/.

56. Silvius, J. R. 1982. Thermotropic phase transitions of pure lipids in model membranes and their modifications by membrane proteins. *In* Lipid-Protein Interactions. P. C. Jost and O. H. Griffith, eds. John Wiley & Sons, pp. 239–281.

Supplemental Information

Membrane Adhesion via Glycolipids Occurs for Abundant Saccharide Chemistries

Victoria M. Latza, Bruno Demé, and Emanuel Schneck

Membrane adhesion via glycolipids occurs for abundant saccharide chemistries

V. M. Latza, B. Demé, and E. Schneck

Supporting Information

1.) Electrostatic repulsion between charged surfaces in a monovalent electrolyte

For weakly charged surfaces in a monovalent electrolyte the pressure Π_{el} associated with the electrostatic repulsion is given as [1]:

$$\Pi_{el}(d_w) \cong 2k_B T \rho_0 [\cosh(e\psi_m(d_w)/k_B T) - 1],$$

where ρ_0 is the number density of monovalent ions in the bulk, e is the electron charge, and ψ_m is the electric potential at the midplane (i.e., the center of the water layer). For sufficiently low charge densities (i.e., in the Debye-Hückel limit) and within the weak-overlap approximation, ψ_m is proportional to the surface electric potential ψ_0:

$$\psi_m(d_w) = 2\psi_0 e^{-\kappa d_w/2},$$

where

$$\kappa^{-1} = \sqrt{\frac{\varepsilon_0 \varepsilon k_B T}{2e^2 \rho_0}}$$

is the Debye length and ψ_0 follows from the surface charge density σ according to the relation

$$\sigma^2 = 2\varepsilon\varepsilon_0 k_B T \sum_j \rho_0 [\exp(-z_j e\psi_0/k_B T) - 1],$$

where $z_j = \pm 1$ is the charge number of the cations and anions, respectively.

2.) Lamellar periodicities obtained by SAXS for of DMPC membranes containing *Psyc-sat* and DMPG

Fig. S1 shows $d(f_{gly})$ for DMPC membranes loaded with *Psyc-sat*, a glycolipid with a mono-galactose headgroup. The lamellar periodicity decreases approximately linearly with increasing f_{gly}. The smallest value is $d \approx 6$ nm at $f_{gly} = 0.2$.

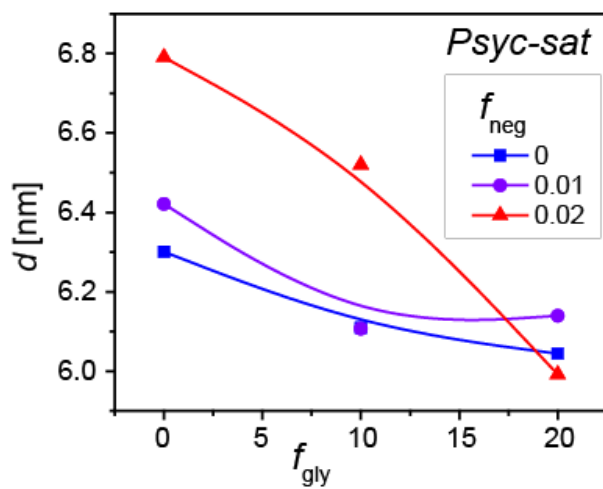**Figure S1:** Lamellar periodicities d obtained by SAXS for DMPC lipid membrane multilayers containing various fractions f_{gly} of *Psyc-sat* and f_{neg} of the negatively charged lipid DMPG. The measurements were conducted at 50 °C. Solid lines are guides to the eye.

3.) Neutron diffraction (ND) measurements under bulk water conditions

The results of ND measurements of POPC membranes loaded with *DGDG-unsat* at f_{gly} = 0.2 and f_{neg} = 0, and of DMPC membranes loaded with *LacCer-sat* at f_{gly} = 0.2 and f_{neg} = 0 under bulk water conditions are summarized in Fig. S2. The intensities of the second Bragg sheets were found to be too weak to be analyzed.
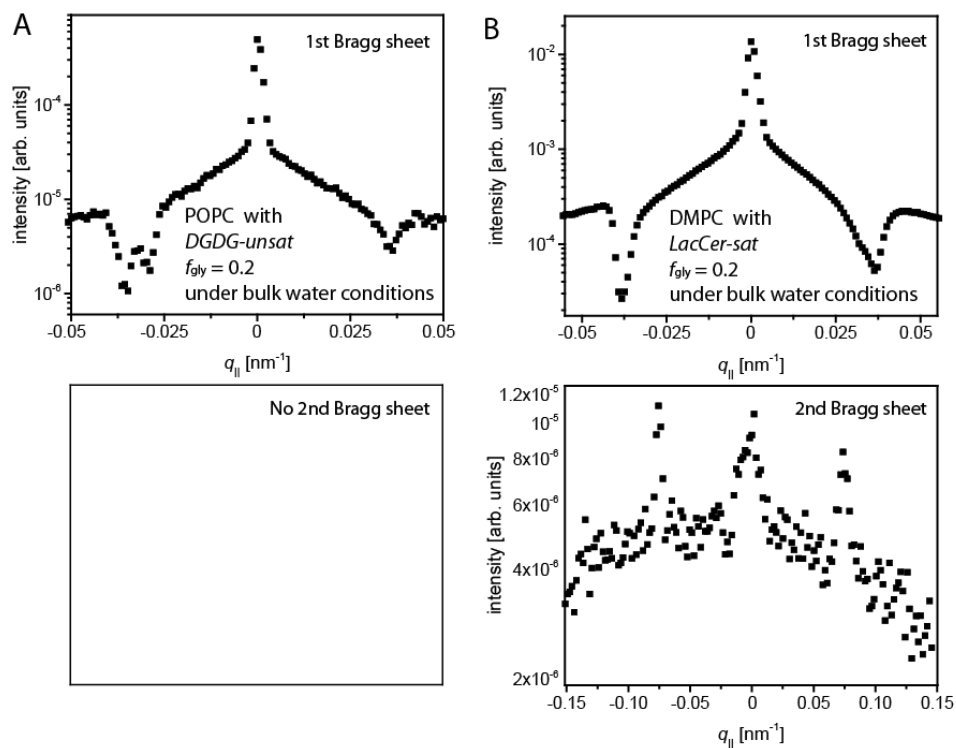

Figure S2: Intensities of the first (top) and second (bottom) Bragg sheets of (A) POPC membranes loaded with *DGDG-unsat* at f_{gly} = 0.2 and f_{neg} = 0 and (B) DMPC membranes loaded with *LacCer-sat* at f_{gly} = 0.2 and f_{neg} = 0, both under bulk water conditions.

4.) Accounting for absorption of the neutron beam in the modeled Bragg sheets

Close to the conditions $\Omega = 0$ and $\Omega = \Gamma$ the incident and scattered neutron beams, respectively, travel essentially parallel to the sample plane and thus get strongly absorbed on the way through the sample. While crystalline silicon is practically transparent to neutrons on the length scales relevant for the present work, beam absorption through incoherent scattering by the lipid layer is considerable, because the lipids are hydrogenous, i.e., they contain light hydrogen (^{1}H). The attenuation coefficient for DMPC (chemical formula: $C_{36}H_{72}NO_8P$) at a mass density of $1\,g\,cm^{-3}$ is $\mu \approx 5\,cm^{-1}$ at $\lambda = 4.518\,\text{Å}$ [2]. Hydrating D_2O has negligible contribution to absorption.

The average thickness of the lipid film on the silicon wafer is $h \approx 1\,\mu m$, as follows from the deposited lipid amount ($\approx 1\,mg$), their mass density ($\approx 1\,g\,cm^{-3}$), as well as from the approximate extensions of the coated region in the direction parallel to the beam ($L_{||} \approx 2\,cm$) and in the perpendicular direction ($L_\perp \approx 5\,cm$). For each coated surface element along the direction of the beam ($0 \le x \le L_{||}$), the maximal path length is $s_{max}^{in}(x) = x$ for the incident beam and $s_{max}^{sc}(x) = L_{||} - x$ for the scattered beam. Depending on the angle of incidence, the actual path length is given as

$$s_{in}(\Omega, x) = MIN\left(\left[s_{max}^{in}(x);\ h/\sin(|\Omega|)\right]\right) \qquad\qquad \text{for the incident beam}$$

and

$$s_{sc}(\Omega, x) = MIN\left(\left[s_{max}^{sc}(x);\ h/\sin(|\Omega - \Gamma|)\right]\right) \qquad\qquad \text{for the scattered beam}$$

The overall attenuation by the sample on the way to the detector, represented as the transmission function $T(\Omega)$ thus follows as $T(\Omega) = T_{in}(\Omega) \cdot T_{sc}(\Omega)$, where

$$T_{in}(\Omega) = \frac{1}{L_{||}} \int_0^{L_{||}} e^{-\mu \cdot s_{in}(\Omega, x)} dx$$

$$T_{sc}(\Omega) = \frac{1}{L_{||}} \int_0^{L_{||}} e^{-\mu \cdot s_{sc}(\Omega, x)} dx$$

5.) Influence of negatively charged phospholipids in the interaction of phospholipid bilayers containing *TetraG-sat*

Fig. S3 shows $d(f_{gly})$ for DPPC membranes loaded with *TetraG-sat*, a glycolipid with a linear tetrasaccharide headgroup composed of (galactose)-(N-acetyl-galactose)-(galactose)-(glucose). There is a strong increase of d with f_{gly}, which is steep in the beginning until it reaches saturation. Incorporation of negatively charged lipids has no pronounced effect in the investigated range ($f_{neg} \leq 0.05$)
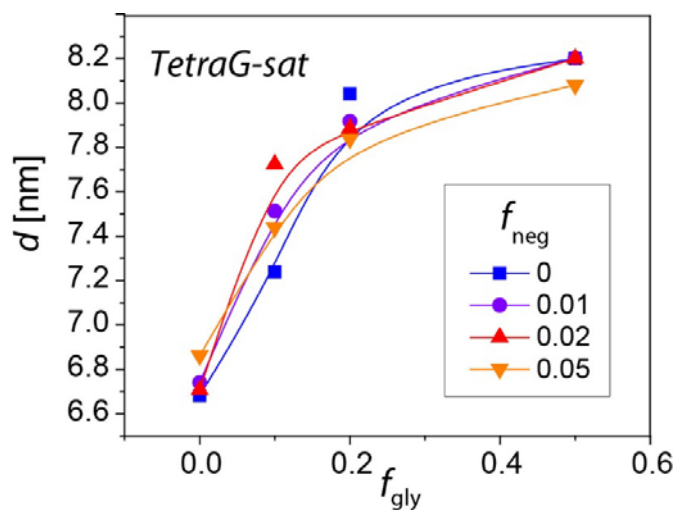

Figure S3: Lamellar periodicities d obtained by SAXS for DPPC lipid membrane multilayers containing various fractions f_{gly} of *TetraG-sat* and f_{neg} of the negatively charged lipid DPPG. The measurements were conducted at 50 °C. Solid lines are guides to the eye.

References

[1] Israelachvili, J. N., *Intermolecular and surface forces*. Academic press: 2011

[2] NIST Center for Neutron Research, https://www.ncnr.nist.gov/resources/activation/